In-plane magnetic response and Maki parameter of alternating-twist multilayers

Igor Vasilevskiy,[1,*] Miguel Sánchez Sánchez,[1] Khadija Challaouy,[2]
Dionisios Margetis,[3] Guillermo Gómez-Santos,[4] and Tobias Stauber[1,†]

[1] *Instituto de Ciencia de Materiales de Madrid, CSIC, E-28049 Madrid, Spain*
[2] *Universidad Internacional Menéndez Pelayo, E-28040 Madrid, Spain*
[3] *Department of Mathematics, and Institute for Physical Science and Technology, University of Maryland, College Park, Maryland 20742, USA*
[4] *Departamento de Física de la Materia Condensada, Instituto Nicolás Cabrera and Condensed Matter Physics Center (IFIMAC), Universidad Autónoma de Madrid, E-28049 Madrid, Spain*

(Dated: March 18, 2026)

We analytically study the orbital response of alternating-twist graphene systems with four and five layers to an in-plane magnetic field, using the unitary transformation introduced by Khalaf et al. [E. Khalaf et al., Phys. Rev. B **100**, 085109 (2019)]. This transformation maps an alternating-twist N-layer system onto $N/2$ decoupled twisted bilayer graphene (TBG) systems with distinct effective twist angles, together with a single decoupled layer for odd N, thereby generating a hierarchy of $N/2$ magic angles. For five layers, we find that the orbital in-plane magnetic response is negligibly small, and we expect this property to hold for all systems with an odd number of layers. For a tetralayer system, we approximately express the in-plane orbital susceptibility in terms of the corresponding TBG responses, which are large compared to the spin susceptibility and even diverge in the clean limit at charge neutrality near the magic angle. Remarkably, the in-plane magnetic response is strongly angle dependent: compared with TBG, it is about 0.01 times smaller at the first magic angle, whereas at the second it reaches about 3.6 times the value of magic-angle TBG. We finally introduce the in-plane Maki parameter as the ratio between the difference in orbital susceptibility of the normal and superconducting states to the paramagnetic Pauli susceptibility. For TBG, we find values up to 2 near the magic angle. Our analysis can be extended to other response functions and suggests that the different effective magic angles in alternating-twist multilayers may even host distinct superconducting phases.

I. INTRODUCTION

The discovery of superconductivity in twisted bilayer graphene [1] at the magic angle (MATBG) has attracted much attention by showing that flat-band engineering can induce unexpected phase transitions [2–33]. The MATBG phase diagram shows notable parallels to what is observed in high-T_c superconductors, with the superconducting dome emerging in close proximity to an insulating phase [34]. Moreover, the notably large ratio between the critical and Fermi temperatures places MATBG within the strong-coupling regime of known superconductors [35, 36].

Superconductivity has since been reported in related graphene moiré systems, which include both commensurate [37–40] and incommensurate structures [41, 42]. In alternating-twist graphene multilayer systems, this behavior is expected because the Hamiltonian can be mapped onto decoupled twisted bilayer graphene (TBG) systems for an even number of layers, and onto decoupled TBG systems plus an additional detached single layer graphene (SLG) for an odd number of layers [43]. This mapping allows one to predict the magic angles, $\theta_{N,m}$, for a higher number of layers, yielding $\theta_{3,m} = \sqrt{2}\theta_m$, $\theta_{4,m} \in \{\varphi\theta_m, \varphi^{-1}\theta_m\}$, and $\theta_{5,m} \in \{\sqrt{3}\theta_m, \theta_m\}$ for $N = 3, 4, 5$, respectively, where θ_m is the TBG magic angle and $\varphi = (1+\sqrt{5})/2$.

Although the systems exhibit certain similarities, the superconducting pairing mechanism may differ. One way to analyze this is by measuring the violation of the Pauli limit. This limit, derived from BCS theory, predicts the critical magnetic field that is needed to break superconductivity by aligning the spins of the two electrons that form the singlet Cooper pair. This Clogston-Chandrasekhar or Pauli limit is given by $B_{\mathrm{P}} = 1.86\,T_{\mathrm{c}}$ (in Tesla for T_{c} in Kelvin) [44, 45].

In typical experiments, the magnetic field is applied in the in-plane direction to avoid additional orbital effects, which vanish in a purely two-dimensional structure. In fact, a violation of the Pauli limit by a factor of 2-3 was found in alternating-twist multilayers with $N = 3, 4, 5$ [46, 47], corroborating the view that superconductivity is unconventional in these systems [48, 49]. This interpretation was ultimately confirmed for the trilayer system through combined tunneling spectroscopy and transport measurements [50].

The in-plane orbital susceptibility of TBG is intrinsically large [51–53], giving rise to exceptionally strong orbital magnetization responses [54] that are highly sensitive to symmetry breaking and valley polarization

* igor.vasilevskiy@csic.es
† tobias.stauber@csic.es

[55]. As a consequence, the orbital contribution dominates over the spin susceptibility of Cooper pairs, so that no direct conclusion on the pairing symmetry can be drawn. In view of the mapping of alternating-twist multilayers onto effective TBG systems, it is therefore somewhat surprising that their in-plane orbital response can be significantly reduced and does not mask the spin susceptibility, particularly in the case with $N = 4$.

In this paper, we analytically study the orbital response of alternating-twist graphene multilayers due to an in-plane magnetic field, primarily focusing on the cases with $N = 4$ and $N = 5$ layers. In addition, we attempt to draw conclusions for alternating-twist systems with a higher number of layers. Our approach is based on the unitary transformation introduced in [43], and extends substantially our previous results on the optical response for the particular case of the alternating-twist trilayer ($N = 3$) [56]. We will also introduce and calculate the in-plane Maki parameter that relates the orbital and spin-susceptibilities.

For trilayers, the small in-plane orbital magnetic response can be attributed to the mirror symmetry of the system [56]. By contrast, multilayers with an even N are not mirror symmetric. At the magic angle regime, one would thus expect a large in-plane orbital magnetic response in such systems. We show that for $N = 4$ this is indeed the case, but only for the magic angle equal to $\varphi^{-1}\theta_m$. However, for the larger magic angle, $\varphi\theta_m$, we find a vanishing in-plane magnetic susceptibility that would allow one to detect the spin-susceptibility of the Cooper pairs, exclusively. As a result, for $N = 4$ the two magic angles exhibit qualitatively distinct magnetic behavior and may support contrasting superconducting properties within the same alternating-twist multilayer system. This result together with the discussion of the in-plane Maki parameter constitutes the main highlights of the present work. For $N = 5$, we analytically verify the expected property that the in-plane orbital magnetic response is negligibly small. More generally, this property should hold for all alternating-twist multilayer systems with an odd number of layers.

The remainder of the paper is organized as follows. In Sec. II, we discuss our approach and introduce the layer-resolved conductivity tensor. We also define the magnetic field and dipole density in terms of layer-contrasted electric fields and currents, respectively. Section III is devoted to the calculation of the in-plane magnetic response. There we express the current response of the multilayer in terms of those of the bilayer and single-layer systems, which gives rise to cross terms that are negligible in the flat-band regime. In Sec. IV, we finally address the superconducting phase and discuss the Pauli-limit and the in-plane Maki parameter. Sec. V summarizes the main findings. The two Appendices present more details on the analytical approach.

II. RESPONSE THEORY FOR MULTILAYERS

The electromagnetic response of layered two-dimensional systems to in-plane electric or magnetic fields can be decomposed into the sheet current responses of the individual layers, extending the approach of Ref. 56. These sheet currents are obtained from the layer-resolved Ohm's law, with dynamical conductivities obtained within linear response. We will argue that the magnitude of the equilibrium response can then be inferred from the static ordered limit $\lim_{\omega\to 0}\lim_{\mathbf{q}\to 0}$ of the dynamical conductivities at charge neutrality. This argument relies on the observation that the equilibrium response, which requires the reverse order of limits, $\lim_{\mathbf{q}\to 0}\lim_{\omega\to 0}$, can be related to the present dynamical calculation, through a "contact term" that only includes contributions from the Fermi surface, see Ref. 57. At charge neutrality, this contact term vanishes, and the two types of limits therefore coincide. Furthermore, we will argue that, for the orbital magnetic susceptibility, the value at charge neutrality becomes representative of the entire band even at finite doping.

Throughout this paper, we argue that the electromagnetic response of the multilayer can be expressed in terms of the response of TBG. For this purpose, we rely on the unitary transformation introduced by Khalaf et al. [43], which maps an alternating-twist multilayer with an even number of layers N onto $N/2$ decoupled twisted bilayers. For TBG, it has been shown that near charge neutrality the magnetic response is approximately constant. Consequently, the magnetic response evaluated at $\mu = 0$ in the present treatment should provide a reliable estimate of the equilibrium response of the multilayer systems considered here. Moreover, it sets the scale for the Fermi surface contribution to the orbital susceptibility, which is always paramagnetic.

We are particularly interested in the in-plane response around the flat-band regime characterized by the magic angles $\theta_{N,m}$. In TBG, the magnetic response in the clean limit at $\mu = 0$ is paramagnetic and diverges algebraically as a function of the twist angle with $(\theta - \theta_m)^{-0.2}$ for $\theta > \theta_m$ [53]. The divergence at the magic angle will be regularized in realistic systems, and we denote the resulting (finite) susceptibility by χ_{TBG}, which will serve as a reference scale for the equilibrium response of the multilayer systems.

A. Layer-resolved Ohm's law and Kubo formula

Ohm's law for the general layer-resolved system in the frequency domain for a system with N layers is

given by [51, 57]

$$\mathbf{J}_\ell = \sum_{\ell'=1}^{N} \boldsymbol{\sigma}^{\ell\ell'} \mathbf{E}_{\ell'} \quad (\ell = 1, \ldots, N) \,, \tag{1}$$

where $\mathbf{J}_\ell$ and $\mathbf{E}_\ell$ denote the macroscopic surface current density and electric field in layer ℓ, respectively. The 2×2 matrices $\boldsymbol{\sigma}^{\ell\ell'}(\omega)$ have elements defined by

$$\sigma^{\ell\ell'}_{\nu\nu'}(\omega) = i \frac{e^2}{\omega + i\delta} \chi^{\ell\ell'}_{\nu\nu'}(\omega + i\delta), \tag{2}$$

with $\delta \downarrow 0$ ensuring a retarded response. The current-current response function reads

$$\chi^{\ell\ell'}_{\nu\nu'}(\omega) = -\frac{i}{\hbar} \int_0^\infty dt \; e^{i\omega t} \langle [j^\ell_\nu(t), j^{\ell'}_{\nu'}(0)] \rangle \,, \tag{3}$$

where $j^\ell_\nu(t)$ is the ν-directed current operator ($\nu = x, y$) at layer ℓ in the interaction picture, and $\langle \cdot \rangle$ denotes the equilibrium average. In the following, we will also sometimes use the shortcut notation $\langle\langle j^\ell_\nu(t), j^{\ell'}_{\nu'} \rangle\rangle = \chi^{\ell\ell'}_{\nu\nu'}$.

Here, we consider moiré multilayers with $N = 4$ and $N = 5$. For the sake of completeness, we will also discuss the results for $N = 3$, presented in Ref. 56. The twist angle of layer ℓ is $\theta(\ell) = (-1)^\ell \theta/2$, where $0 < \theta < \pi/2$ and $\ell = 1, \ldots, N$; and the interlayer distance is $a = 3.4\,\text{Å}$.

The alternating-twist geometry imposes certain symmetries on the total conductivity. The 2×2 matrices connecting layers with the same twist angle will be proportional to the identity matrix:

$$\boldsymbol{\sigma}^{\ell(\ell+2n)} = \sigma_0^{\ell(\ell+2n)} \mathbf{1} \,, \; \ell + 2n \leq N, \tag{4}$$

where $\sigma_0^{\ell\ell'}$ is the longitudinal conductivity. Chirality is encoded in the off-diagonal entries of the non-local matrices:

$$\boldsymbol{\sigma}_\pm^{\ell(\ell+2n+1)} = \sigma_0^{\ell(\ell+2n+1)} \mathbf{1} \pm i \sigma_{xy}^{\ell(\ell+2n+1)} \boldsymbol{\tau}_y, \quad \ell + 2n + 1 \leq N, \tag{5}$$

where $\boldsymbol{\tau}_y$ denotes the y-Pauli matrix. Moreover, time-reversal symmetry implies $\sigma^{\ell\ell'}_{\nu\nu'} = \sigma^{\ell'\ell}_{\nu'\nu}$.

The total conductivity matrix for the trilayer system then reads [56]

$$\sigma_{\text{tot}} = \begin{pmatrix} \boldsymbol{\sigma}^{11} & \boldsymbol{\sigma}^{12}_+ & \boldsymbol{\sigma}^{13} \\ \boldsymbol{\sigma}^{12}_- & \boldsymbol{\sigma}^{22} & \boldsymbol{\sigma}^{12}_- \\ \boldsymbol{\sigma}^{13} & \boldsymbol{\sigma}^{12}_+ & \boldsymbol{\sigma}^{11} \end{pmatrix} \,. \tag{6}$$

For $N = 4$, this matrix becomes

$$\sigma_{\text{tot}} = \begin{pmatrix} \boldsymbol{\sigma}^{11} & \boldsymbol{\sigma}^{12}_+ & \boldsymbol{\sigma}^{13} & \boldsymbol{\sigma}^{14}_+ \\ \boldsymbol{\sigma}^{12}_- & \boldsymbol{\sigma}^{22} & \boldsymbol{\sigma}^{23}_- & \boldsymbol{\sigma}^{13}_+ \\ \boldsymbol{\sigma}^{13} & \boldsymbol{\sigma}^{23}_+ & \boldsymbol{\sigma}^{22}_- & \boldsymbol{\sigma}^{12}_+ \\ \boldsymbol{\sigma}^{14}_- & \boldsymbol{\sigma}^{13}_+ & \boldsymbol{\sigma}^{12}_- & \boldsymbol{\sigma}^{11} \end{pmatrix} \,. \tag{7}$$

For $N = 5$, we have

$$\sigma_{\text{tot}} = \begin{pmatrix} \boldsymbol{\sigma}^{11} & \boldsymbol{\sigma}^{12}_+ & \boldsymbol{\sigma}^{13} & \boldsymbol{\sigma}^{14}_+ & \boldsymbol{\sigma}^{15} \\ \boldsymbol{\sigma}^{12}_- & \boldsymbol{\sigma}^{22} & \boldsymbol{\sigma}^{23}_- & \boldsymbol{\sigma}^{24} & \boldsymbol{\sigma}^{14}_- \\ \boldsymbol{\sigma}^{13} & \boldsymbol{\sigma}^{23}_+ & \boldsymbol{\sigma}^{33} & \boldsymbol{\sigma}^{23}_+ & \boldsymbol{\sigma}^{13} \\ \boldsymbol{\sigma}^{14}_- & \boldsymbol{\sigma}^{24} & \boldsymbol{\sigma}^{23}_- & \boldsymbol{\sigma}^{22} & \boldsymbol{\sigma}^{12}_- \\ \boldsymbol{\sigma}^{15} & \boldsymbol{\sigma}^{14}_+ & \boldsymbol{\sigma}^{13} & \boldsymbol{\sigma}^{12}_+ & \boldsymbol{\sigma}^{11} \end{pmatrix} \,. \tag{8}$$

One can see that the alternating-twist geometry and time-reversal symmetry constrain the layer-resolved conductivity, reducing it to a limited number of independent response functions, i.e., 4, 6 and 9 for $N = 3, 4, 5$ respectively.

B. Electric and magnetic fields

Until now, we have only considered Ohm's law involving layer-resolving sheet current densities and electric fields. We can now define the average electric field

$$\mathbf{E}^\parallel = \frac{1}{N} \sum_{\ell=1}^{N} \mathbf{E}_\ell \,. \tag{9}$$

In order to define the layer differences, we will introduce magnetic quantities by discretizing the two equations $-\partial_t \mathbf{B} = \nabla \times \mathbf{E} \to \partial_z \mathbf{e}_z \times \mathbf{E}$ and $\mathbf{j} = \nabla \times \mathbf{m} \to \partial_z \mathbf{e}_z \times \mathbf{m}$. From the discrete (layer-resolved) version of the Maxwell-Faraday law we get the following relations for the average magnetic field between layers ℓ and ℓ':

$$i\omega a(\ell - \ell') \mathbf{B}^\parallel_{\ell\ell'} = \mathbf{e}_z \times (\mathbf{E}_\ell - \mathbf{E}_{\ell'}) \,. \tag{10}$$

Note that a constant in-plane magnetic field within the sample is given by $\mathbf{B}^\parallel = \mathbf{B}^\parallel_{(\ell+1)\ell}$ for $\ell = 1, \ldots, N-1$. The electric fields must thus linearly increase as a function of the layer index, ℓ.

C. Electric and magnetic dipoles

Let us now turn to the in-plane sheet currents induced by the external fields. These currents give rise to electric and magnetic moments, and the total current density can be related to the electric polarization by

$$-\partial_t \mathbf{p} = \mathbf{J}_{\text{tot}} = \sum_{\ell=1}^{N} \mathbf{J}_\ell \,. \tag{11}$$

Furthermore, in Ref. 56, we outlined that the sheet current densities can be written as

$$\mathbf{J}_\ell = \frac{\mathbf{J}_{\text{tot}}}{N} + \mathbf{j}_\ell \,, \tag{12}$$

where $\mathbf{J}_{\text{tot}} = \sum_\ell \mathbf{J}_\ell$ denotes the total current and $\mathbf{j}_\ell$ the deviation from the average. Since $\sum_\ell \mathbf{j}_\ell = 0$, each

$\mathbf{j}_\ell$ can be considered as the sum of the magnetization currents associated with the regions above ($\mathbf{m}_\ell$) and below ($\mathbf{m}_{\ell-1}$) the layer ℓ. For $\ell = 1, \ldots, N$ we get

$$\mathbf{m}_{\ell-1} - \mathbf{m}_\ell = a(\mathbf{e}_z \times \mathbf{j}_\ell)\,, \tag{13}$$

with the constraints $\sum_\ell \mathbf{j}_\ell = 0$ and $\mathbf{m}_0 = \mathbf{m}_N = 0$. Eq. (13) provides the set of magnetizations $\{\mathbf{m}_\ell\}$ associated to any set of currents $\{\mathbf{j}_\ell\}$, and vice versa. The total magnetic moment per unit area $\mathbf{M} = \sum_{\ell=1,\ldots,N-1} \mathbf{m}_\ell$ is thus given by

$$\mathbf{M} = a \sum_{\ell=1}^{N} \frac{2\ell - N - 1}{2} (\mathbf{e}_z \times \mathbf{j}_\ell)\,. \tag{14}$$

The in-plane magnetic response is thus generated by layer-dependent current imbalances and encodes the spatial distribution of magnetization across the multilayer stack.

III. IN-PLANE MAGNETIC RESPONSE

We now turn our attention to the in-plane magnetic response of alternating-twist multilayer systems. As shown in Sec. II B, an in-plane magnetic field emerges from the layer-discriminated electric field in the form

$$\mathbf{E}_B^N = \mathbf{E}_0 \sum_{\ell=1}^{N} \frac{2\ell - N - 1}{2} \mathbf{e}_\ell\,, \tag{15}$$

where $\mathbf{e}_\ell$ denotes any vector in the basis of the layer space. The magnitude B of the magnetic field is thus given by the relation $i\omega a B = E_0$.

In the remainder of this section, we will discuss the in-plane magnetic response of tetralayer ($N = 4$) and pentalayer ($N = 5$) systems. For completeness, we also briefly review the trilayer case ($N = 3$), derived in our previous work. To be more general, we will denote the in-plane current operator by two sub-indices, $\mathbf{J}_\ell \to \mathbf{j}_{\ell\ell}$ in order to also discuss "vertical" current densities $\mathbf{j}_{\ell\ell'}$ with $\ell \neq \ell'$; see Appendix A. Since the magnetic response is always parallel or antiparallel to the applied magnetic field, we will suppress the boldface vector notation when the symbolism can be self evident.

A. Trilayer response

Following Ref. [56], the total magnetic moment per unit area for $N = 3$ reads

$$\mathbf{M} = 2i\omega a^2 (\sigma_0^{11} - \sigma_0^{13})\mathbf{B}\,. \tag{16}$$

The "counterflow" between the first and the third layer only involves a cross term, $\sigma_c^1 = 2(\sigma_0^{11} - \sigma_0^{13})$, related to the layer-resolved current-current correlators as

$$\sigma_c^1 = \langle\langle \bar{j}_{13}\bar{j}_{31} + \bar{j}_{31}\bar{j}_{13}\rangle\rangle\,, \tag{17}$$

by use of the transformed current operators $\bar{j}_{\ell\ell'}$; see Ref. [56] and Appendix A.

Because of the kinematic constraints arising from the large mismatch between the Fermi velocities of the effective TBG and the decoupled SLG bands, this contribution, σ_c^1, is expected to be negligibly small. In the same work [56], it was analytically shown that σ_c^1 is in fact comparable to, or smaller than, the corresponding atomistic (lattice) effect in SLG.

B. Tetralayer response

By applying the electric field of Eq. (15) to the system with $N = 4$ layers, we obtain the following relations for the currents:

$$j_{44} = \frac{E_0}{2}\left[3(\sigma_0^{11} - \sigma_0^{14}) + (\sigma_0^{12} - \sigma_0^{13})\right] = -j_{11}\,, \tag{18}$$

$$j_{33} = \frac{E_0}{2}\left[3(\sigma_0^{12} - \sigma_0^{13}) + (\sigma_0^{22} - \sigma_0^{23})\right] = -j_{22}\,, \tag{19}$$

where the conductivities have been reduced to the independent response functions dictated by the symmetry structure of Eq. (7). Given that $i\omega a B = E_0$ and $\mathbf{m}_\ell = \chi_\ell \mathbf{B}$ (where $B = |\mathbf{B}|$), we obtain

$$\chi_1 = i\omega \frac{a^2}{2}\left[3(\sigma_0^{11} - \sigma_0^{14}) + (\sigma_0^{12} - \sigma_0^{13})\right] = \chi_3\,, \tag{20}$$

$$\chi_2 = i\omega \frac{a^2}{2}\Big[3(\sigma_0^{11} - \sigma_0^{14}) + 4(\sigma_0^{12} - \sigma_0^{13}) + (\sigma_0^{22} - \sigma_0^{23})\Big]\,. \tag{21}$$

After transforming the tetralayer into a system of two effective TBG systems, the layer-resolved conductivities can be rewritten in the corresponding basis; see Appendix B 1. Using the notation of Ref. 51, we define

$$\sigma_0^1 = \langle\langle \bar{j}_{11}\bar{j}_{11}\rangle\rangle = \langle\langle \bar{j}_{22}\bar{j}_{22}\rangle\rangle\,, \tag{22}$$

$$\sigma_0^2 = \langle\langle \bar{j}_{33}\bar{j}_{33}\rangle\rangle = \langle\langle \bar{j}_{44}\bar{j}_{44}\rangle\rangle\,, \tag{23}$$

$$\sigma_1^1 = \langle\langle \bar{j}_{11}\bar{j}_{22}\rangle\rangle = \langle\langle \bar{j}_{22}\bar{j}_{11}\rangle\rangle\,, \tag{24}$$

$$\sigma_1^2 = \langle\langle \bar{j}_{33}\bar{j}_{44}\rangle\rangle = \langle\langle \bar{j}_{44}\bar{j}_{33}\rangle\rangle\,. \tag{25}$$

Additionally, we also have to introduce the response that couples the two effective bilayer systems as follows:

$$\sigma_c^1 = \langle\langle \bar{j}_{13}\bar{j}_{31} + \bar{j}_{31}\bar{j}_{13}\rangle\rangle\,, \tag{26}$$

$$\sigma_c^2 = \langle\langle \bar{j}_{24}\bar{j}_{42} + \bar{j}_{42}\bar{j}_{24}\rangle\rangle\,, \tag{27}$$

$$\sigma_c^3 = \langle\langle \bar{j}_{13}\bar{j}_{42} + \bar{j}_{31}\bar{j}_{24}\rangle\rangle = \langle\langle \bar{j}_{24}\bar{j}_{31} + \bar{j}_{42}\bar{j}_{13}\rangle\rangle\,. \tag{28}$$

The final expressions for the conductivities $\sigma_0^{\ell\ell'}$ can be found in Appendix B 1. The response functions can

now be written as

$$\chi_1 = i\omega\frac{a^2}{10}\Big[(3\varphi^{-2}-1)(\sigma_0^1-\sigma_1^1) + (3\varphi^2-1)(\sigma_0^2-\sigma_1^2)+4(\sigma_c^1+\sigma_c^3)\Big], \quad (29)$$

$$\chi_2 = i\omega\frac{a^2}{10}\Big[(3\varphi^{-2}-4+\varphi^2)(\sigma_0^1-\sigma_1^1) + (3\varphi^2-4+\varphi^{-2})(\sigma_0^2-\sigma_1^2) + 7(\sigma_c^1+\sigma_c^3)+(\sigma_c^2+\sigma_c^3)\Big], \quad (30)$$

where $\varphi = (1+\sqrt{5})/2$.

1. System response near the first magic angle

Let us now discuss the behavior of this system when the first effective bilayer is close to the respective magic angle. The renormalized Fermi velocities of the two effective systems, $v_{\rm F}^j$, are then very different at the K-point, $v_{\rm F}^2 \gg v_{\rm F}^1$. The coupling terms $\sigma_c^1+\sigma_c^3$ are thus expected to be relatively small because of the restricted phase space. The counter-flow term $\sigma_0^2-\sigma_1^2$ also becomes negligible as the second effective bilayer is away from its magic angle regime. With respect to the susceptibility of the TBG, $\chi_{\rm TBG} = i\omega(a^2/2)(\sigma_0-\sigma_1)$, we can thus approximate

$$\chi_1/\chi_{\rm TBG} = \frac{1}{5}(3\varphi^{-2}-1) \approx 0.03\,, \quad (31)$$

$$\chi_2/\chi_{\rm TBG} = \frac{1}{5}(3\varphi^{-2}-4+\varphi^2) \approx -0.05\,. \quad (32)$$

By adding the susceptibilities of the three magnetizations, $\chi = 2\chi_1+\chi_2$, with $\mathbf{M} = \chi\mathbf{B}$, we obtain

$$\chi/\chi_{\rm TBG} = \frac{1}{5}(9\varphi^{-2}-6+\varphi^2) \approx 0.01\,. \quad (33)$$

This estimated value is one of the main findings of our paper, and shows that the orbital in-plane magnetic response is negligible at the larger magic angle, $\theta_{4,m}^1 = \varphi\theta_m$.

2. System response near the second magic angle

The analysis proceeds analogously to the previous case (Sec. III B 1) when the second effective bilayer system is tuned close to its magic angle, $\theta_{4,m}^2 = \varphi^{-1}\theta_m$. The renormalized Fermi velocities at the K point are strongly different, but now with $v_{\rm F}^1 \gg v_{\rm F}^2$. The coupling terms $\sigma_c^1+\sigma_c^3$ are once again expected to be small because of the restricted phase space. The counter-flow contribution $\sigma_0-\sigma_1$ of the first system can likewise be neglected, i.e., $|\sigma_0^1-\sigma_1^1| \ll |\sigma_0^2-\sigma_1^2|$. In regard to the susceptibility of the TBG, $\chi_{\rm TBG} = i\omega(a^2/2)(\sigma_0-\sigma_1)$, we can thus approximate

$$\chi_1/\chi_{\rm TBG} = \frac{1}{5}(3\varphi^2-1) \approx 1.4\,, \quad (34)$$

$$\chi_2/\chi_{\rm TBG} = \frac{1}{5}(3\varphi^2-4+\varphi^{-2}) \approx 0.8\,. \quad (35)$$

By adding the susceptibilities of the three magnetizations according to $\chi = 2\chi_1+\chi_2$, we finally obtain

$$\chi/\chi_{\rm TBG} = \frac{1}{5}(9\varphi^2-6+\varphi^{-2}) \approx 3.6\,. \quad (36)$$

Note that this approximate value is close to 3, which is what one would obtain by naively adding three twisted-bilayer susceptibilities, since the tetralayer system thickness amounts to three interlayer spacings.

C. Pentalayer response

By applying the electric field of Eq. (15) to the system with $N=5$ layers, while bearing in mind the symmetries of Eq. (8), we obtain the following expressions for the layer currents $\mathbf{J}_\ell \to \mathbf{j}_{\ell\ell}$:

$$j_{55} = \left[2(\sigma_0^{11}-\sigma_0^{15})+(\sigma_0^{12}-\sigma_0^{14})\right]E_0 = -j_{11}\,, \quad (37)$$

$$j_{44} = \left[2(\sigma_0^{12}-\sigma_0^{14})+(\sigma_0^{22}-\sigma_0^{24})\right]E_0 = -j_{22}\,, \quad (38)$$

and $j_{33}=0$. In view of the relation $i\omega aB = E_0$, the susceptibilities read

$$\chi_1 = i\omega a^2\Big[2(\sigma_0^{11}-\sigma_0^{15})+(\sigma_0^{12}-\sigma_0^{14})\Big] = \chi_4, \quad (39)$$

$$\chi_2 = i\omega a^2\Big[2(\sigma_0^{11}-\sigma_0^{15})+3(\sigma_0^{12}-\sigma_0^{14}) + (\sigma_0^{22}-\sigma_0^{24})\Big] = \chi_3. \quad (40)$$

After transforming the pentalayer system into two effective TBG systems and one decoupled effective single-layer, we can rewrite the layer-resolved conductivities in the corresponding basis (see Appendix B 2). It follows that the susceptibilities depend only on the cross terms and are given by

$$\chi_1 = i\omega\frac{a^2}{6}\left[2\sigma_c^1+4\sigma_c^4+\sqrt{3}\sigma_c^5\right]\,, \quad (41)$$

$$\chi_2 = i\omega\frac{a^2}{6}\left[2\sigma_c^1+4\sigma_c^4+3\sqrt{3}\sigma_c^5+3\sigma_c^2\right]\,. \quad (42)$$

This confirms that the in-plane orbital magnetic response of the pentalayer is negligible, relying on the phase space argument for very different Fermi velocities. This behavior closely parallels that of the trilayer system, where the susceptibility also arises solely from cross terms. We expect this feature to generalize to multilayer systems with an odd number of layers.

D. Discussion

For an odd number of layers, $N = 3$ and 5, we have found a relatively small magnetic in-plane response that is independent of the twist angle. Interestingly, regarding the case with $N = 4$ layers and for the larger magic angle related to φ, we find a magnetic response that is 100 times smaller than that of TBG. Moreover, the magnetization changes sign within the tetralayer, as illustrated in Fig. 1 (A). Hence, there must be a small region between layers 2 and 3 where the magnetization becomes zero. This finding is in stark contrast to the prediction that the susceptibility of the tetralayer at the second magic angle is always paramagnetic; see Fig. 1 (B). In this case, the spin susceptibility should be superimposed on a strong orbital contribution, since the average susceptibility is large and comparable to that of TBG.

Our results suggest that the response at the various magic angles of the same multilayer system can be quite different. This behavior might also affect the superconducting pairing instability. In Sec. IV, we will explicitly address the superconducting phase and show that our conclusions remain valid in that regime.

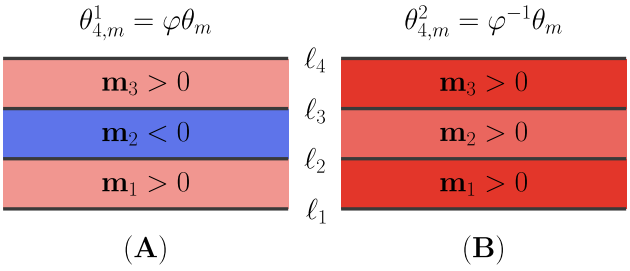

FIG. 1. Schematic of the magnetization profile induced by an in-plane magnetic field in a tetralayer system near the first (A) and second (B) magic angles. The color scale indicates the sign and relative magnitude of the magnetization in each interlayer region.

IV. IN-PLANE MAKI PARAMETER

So far, we have implicitly assumed the multilayer system to be in the normal state. The aforementioned results of our treatment, however, have implications for the superconducting state. In this case, the "contact term" vanishes independently of the filling factor due to the absence of a Fermi surface, i.e., as a consequence of the opening of a superconducting gap. As a result, the equilibrium and Drude-like responses are equivalent [58], and the in-plane magnetic response becomes diamagnetic at sufficiently large doping [51, 57]. Nevertheless, such diamagnetic contribution is also present in the normal phase [44], leaving the Fermi surface contribution as the dominant difference between normal and superconducting phases. For dopings within the flat-band regime, the overall magnitude of such contribution is still set by the value at $\mu = 0$ of the equilibrium response, $\chi_{\rm TBG}$, which is calculated in Sec. III. Therefore, our existing calculation already allows us to draw conclusions on the possibility of extracting the spin susceptibility of Cooper pairs in typical experiments, $\chi_{\rm Cooper}$, depending on whether the condition $\chi_{\rm TBG} \ll \chi_{\rm Cooper}$ is satisfied or not. Next, for the sake of completeness, we explicitly address the equilibrium response and associated Fermi surface contribution.

A. Pauli limit and corrections

The Pauli limit is related to the magnetic field that converts the superconducting phase into the normal phase. It is usually assumed that the only contribution to the magnetic susceptibility is given by the spin response. This has been obtained [44] by equating the energies of the normal and superconducting phases in a magnetic field, in the absence of any Meissner effect. Nominally, in the case with an in-plane magnetic field in a planar system, this energy balance reads

$$\mathcal{F}_N - \frac{1}{2}\chi_{\rm P}^N B_{\rm P}^2 = \mathcal{F}_S - \frac{1}{2}\chi_{\rm P}^S B_{\rm P}^2, \tag{43}$$

where $\mathcal{F}_{N,S}$ is the free energy of the normal (N) or the superconducting (S) phase, and $\chi_{\rm P}^{N,S}$ is the corresponding spin (Pauli) magnetic susceptibility. Under the stated assumptions, only the normal phase has spin susceptibility: $\chi_{\rm P}^N - \chi_{\rm P}^S = \chi_{\rm P}^N = \chi_{\rm P}$, the standard Pauli spin susceptibility of the normal metal, $\chi_{\rm P}$. Thus, we have

$$\mathcal{F}_N - \mathcal{F}_S = \frac{1}{2}\chi_{\rm P} B_{\rm P}^2. \tag{44}$$

Therefore, for the singlet Cooper pairs of the standard BCS-theory, one obtains $B_{\rm P} = 1.86 T_{\rm c}$ (where $B_{\rm P}$ is in Tesla if $T_{\rm c}$ is in Kelvin).

The measurement of the critical magnetic field is not directly linked to the spin-susceptibility if there is also an orbital contribution to the magnetic susceptibility, which is different for the normal and superconducting states. Accordingly, Eq. (43) should be amended to account for the critical magnetic field, $B_{\rm c}$, that bridges the difference in the free energy between the superconducting and normal phases:

$$\mathcal{F}_N - \mathcal{F}_S = \frac{1}{2}(\chi_{\rm P} + \Delta\chi_{\rm orb}) B_{\rm c}^2, \tag{45}$$

with $\Delta\chi_{\rm orb} = \chi_{\rm orb}^N - \chi_{\rm orb}^S$, the difference between the orbital susceptibility of normal and superconducting phases. This difference is given by a Fermi surface contribution, as we will now discuss in detail.

In general, the equilibrium response of the quantity A to a perturbation $V = -\lambda C$, to linear order in the parameter λ, is given by the susceptibility

$$\chi_{AC} = -\langle\langle A, C\rangle\rangle + \frac{1}{S}\sum_{\boldsymbol{k},n}\langle \boldsymbol{k}, n|A|\boldsymbol{k}, n\rangle\langle \boldsymbol{k}, n|C|\boldsymbol{k}, n\rangle\delta(\epsilon_{\rm F} - \epsilon_{\boldsymbol{k},n}) \,, \tag{46}$$

where $\boldsymbol{k}, n$ denote the Bloch momentum and the band number, respectively, $\epsilon_{\rm F}$ is the Fermi energy, and S is the sample surface. The parameter χ_{AC} is the equilibrium (at $\omega = 0$, as $\mathbf{q} \to 0$) response whereas $-\langle\langle A, C\rangle\rangle$ is shorthand notation for the Kubo-like response ($\mathbf{q} = 0$, $\omega \to 0$), already considered in this paper (see, for instance, Eq. (3) where current operators replace the A, C of our discussion here). In our case, $A = C = m_x$, the in-plane magnetic moment in, say, the x-direction, with $\lambda = B_x$, the external magnetic field.

In the superconducting phase, there is no Fermi surface and the equilibrium function is equal to the response from the Kubo formula [58]. The latter, $\langle\langle A, C\rangle\rangle$ in Eq. (46), is the same in the normal and superconducting phases up to corrections of orders of Δ/W, the superconducting order parameter over the band width, which we neglect. Therefore, only the Fermi surface term survives in Eq. (46), as the dominant difference between superconducting and normal phases. In the remainder of this section, we estimate this contribution for the bilayer, trilayer, tetralayer, and pentalayer systems.

B. Bilayer systems

As mentioned above, the difference between normal and superconducting orbital susceptibilities corresponds to the last term of Eq. (46) with $A = C = m_x$, the in-plane orbital magnetic moment. For bilayer systems (BL), this term can be written as

$$\Delta\chi_{\rm orb}^{\rm TBG} = a^2 D_{\rm mag}/2 \,, \tag{47}$$

with

$$D_{\rm mag} = \frac{g_s e^2}{S}\sum_{\boldsymbol{k},n}\langle \boldsymbol{k}, n|j_{11}|\boldsymbol{k}, n\rangle \times \langle \boldsymbol{k}, n|j_{11} - j_{22}|\boldsymbol{k}, n\rangle\delta(\epsilon_{\rm F} - \epsilon_{\boldsymbol{k},n}) \,. \tag{48}$$

Note that $D_{mag} \geq 0$ since $2\langle \boldsymbol{k}, n|j_{11}|\boldsymbol{k}, n\rangle\langle \boldsymbol{k}, n|j_{11} - j_{22}|\boldsymbol{k}, n\rangle = \langle \boldsymbol{k}, n|j_{11} - j_{22}|\boldsymbol{k}, n\rangle\langle \boldsymbol{k}, n|j_{11} - j_{22}|\boldsymbol{k}, n\rangle$.

Equation (45) can now be written as

$$\mathcal{F}_N - \mathcal{F}_S = \frac{1}{2}\chi_{\rm P}(1 + \alpha_{\rm M})B_{\rm c}^2, \tag{49}$$

where we have introduced the *in-plane* Maki parameter (not to be confused with the original *out-of-plane* Maki parameter [60]),

$$\alpha_{\rm M} = \frac{\Delta\chi_{\rm orb}}{\chi_{\rm P}}, \tag{50}$$

as a measure of the orbital modification of the usual Pauli limit.

By using the Pauli susceptibility $\chi_{\rm P} = 2\mu_{\rm B}^2\rho(\epsilon_{\rm F})$ with the Bohr magneton $\mu_{\rm B} = e\hbar/2m_e$ and the density of states (DOS) per spin-channel, $\rho(\epsilon_{\rm F}) = \frac{1}{S}\sum_{\boldsymbol{k},n}\delta(\epsilon_{\rm F} - \epsilon_{\boldsymbol{k},n})$, we obtain

$$\alpha_{\rm M} = \left(\frac{aa_0{\rm eV}}{\alpha a_B\hbar c}\right)^2\frac{\tilde{D}_{\rm mag}}{\tilde{\rho}} = 1.16\frac{\tilde{D}_{\rm mag}}{\tilde{\rho}}, \tag{51}$$

where α is the fine-structure constant ($\alpha = 1/137$), $a_{\rm B}$ is the Bohr radius ($a_{\rm B} = 0.529$Å), the lattice constant is $a_0 = 2.46$Å, and c is the speed of light. We further have $D_{\rm mag} = \tilde{D}_{\rm mag}(e/\hbar)^2{\rm eV}$ and $\rho = \tilde{\rho}(a_0^2{\rm eV})^{-1}$.

The left-hand side of Fig. 2 shows $D_{\rm mag}$ (black) and the density of states of the TBG obtained from the non-interacting tight-binding model at the twist angles $\theta = 1.25°$ (upper panel) and $\theta_m = 1.05°$ (lower panel) using the parameters of Ref. [59]. The right-hand side of Fig. 2 shows the in-plane Maki parameter defined in Eq. (51). In the magic angle regime, the Maki parameter is of the order of unity and can reach values up to 2 throughout the valence band. Hence, the critical in-plane magnetic field that breaks superconductivity is greatly modified from its standard Pauli (spin) value due to the orbital magnetic contribution.

Let us finally note that we can also define an effective magnetic moment for the Bloch electrons $\mu_{\rm orb}$ as Eq.

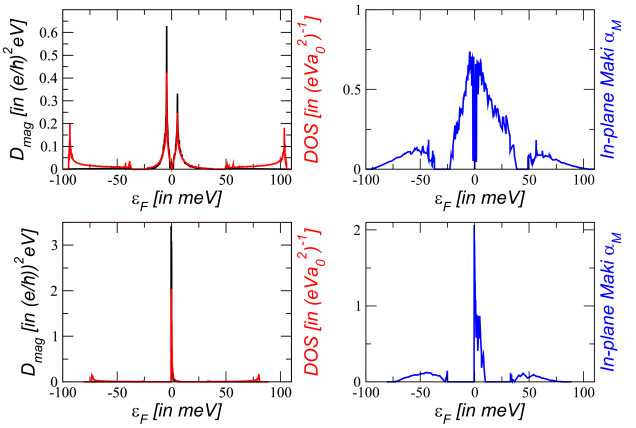

FIG. 2. Left-hand side: The orbital magnetic contribution of Eq. (47) (black) and the density of states of twisted bilayer graphene obtained from the non-interacting tight-binding model at a twist angle $\theta = 1.25°$ (upper panel) and $\theta_m = 1.05°$ (lower panel), using the parameters of Ref. [59]. Right-hand side: The in-plane Maki parameter as defined in Eq. (51).

(48) is a Fermi surface property. This gives

$$\mu_{\rm orb} = \alpha_{\rm M}\mu_{\rm B} \ . \tag{52}$$

Our numerical analysis of $\mu_{\rm orb} \approx 2\mu_{\rm B}$ for valence-band electrons at the magic angle agrees well with the estimate of Ref. [55].

C. Trilayer and Pentalayer systems

For a multilayer with an odd number of layers ($N = 3, 5$), the orbital susceptibility is identically zero, because only the cross terms contribute to the in-plane magnetic response. These cross terms vanish identically due to particle conservation in the two decoupled subsystems. This property is consistent with the fact that the Pauli-limit violation can be directly linked to the spin-susceptibility of the Cooper pairs.

D. Tetralayer systems

Following the above reasoning, for $N = 4$ layers we obtain

$$\begin{aligned}\Delta\chi_{\rm orb}^{\rm TTG} = \frac{a^2}{2}\frac{g_s e^2}{S}\sum_{\boldsymbol{k},n}\Big[&9\langle j_{11}\rangle(\langle j_{11}\rangle - \langle j_{44}\rangle)\\ &+ 6\langle j_{11}\rangle(\langle j_{22}\rangle - \langle j_{33}\rangle)\\ &+ \langle j_{22}\rangle(\langle j_{22}\rangle - \langle j_{33}\rangle)\Big]\delta(E_{\rm F} - \epsilon_{\boldsymbol{k},n}) \ . \end{aligned}\tag{53}$$

where we suppressed the dependence on the quantum numbers in the brackets.

The spectrum of the tetralayer system (TTG) is the sum of the spectra of the two effective bilayer systems (TBG). Therefore, together with the transformation of the current operator, Eq. (53) can be approximately mapped onto the orbital contribution of the bilayer systems, Eq. (47). For this mapping, we assume large counterflow close to the magic angle, first discussed in Ref. [3], and only retain quadratic contributions. It is worthwhile noting that the cross terms now vanish identically.

By these approximations, we obtain the same expressions as in Sec. III, which read

$$\begin{aligned}\frac{\Delta\chi_{\rm orb}^{\rm TTG}}{\Delta\chi_{\rm orb}^{\rm TBG}} &= \frac{1}{5}(9\varphi^{-2} - 6 + \varphi^2) \approx 0.01 \ , \text{ if } \theta \sim \theta_{4,m}^1,\\ \frac{\Delta\chi_{\rm orb}^{\rm TTG}}{\Delta\chi_{\rm orb}^{\rm TBG}} &= \frac{1}{5}(9\varphi^{2} - 6 + \varphi^{-2}) \approx 3.6 \ , \text{ if } \theta \sim \theta_{4,m}^2.\end{aligned}$$

This result clearly shows that the standard value of the Pauli limit only holds for the first magic angle and not for the second one, as the in-plane Maki parameter at hole doping would be $\alpha_{\rm M} \approx 0.02$ and $\alpha_{\rm M} \approx 7$ for the two respective magic angles.

V. SUMMARY

In this paper, we have analytically studied the orbital in-plane magnetic response of alternating-twist graphene multilayers with $N = 4, 5$ layers, extending substantially our previous analysis for the alternating-twist trilayer graphene system [56]. By use of the unitary transformation that block-diagonalizes the Hamiltonian into two effective TBG systems [43], we have been able to estimate the magnetic response from the knowledge of the original TBG system. We have concluded that multilayer systems with an odd number of layers exhibit only a very weak magnetic response.

In contrast, for a system with an even number of layers, specifically for $N = 4$, a strong magnetic response could be expected. However, the behavior of the response at the two magic angles is markedly different. At the first magic angle, $\theta_{4,m}^1 \approx 1.70°$, the magnetization is small, and a sign change in the susceptibility across the central layers leads to regions with vanishing magnetization around layers 2 and 3. At the second magic angle, $\theta_{4,m}^2 \approx 0.65°$, the magnetization points uniformly in the same direction as the magnetic field and reaches a magnitude comparable to that of TBG.

We also introduced and studied the in-plane Maki parameter, $\alpha_{\rm M}$, as a measure of the relative importance of the orbital magnetic susceptibility in the modification of the standard Pauli (spin) limit of superconductivity. Notably, we obtained values up to 2 for $\alpha_{\rm M}$ at the magic angle for the TBG. We argued that this result can also be used for the tetralayer system, and obtained $\alpha_{\rm M} \approx 0.02$ and $\alpha_{\rm M} \approx 7$ for twist angles around the larger and smaller magic angle, respectively.

Our results motivate further studies on the electromagnetic response of twisted multilayer graphene systems. Firstly, the intrinsic chirality of tetralayers may give rise to novel effects. Moreover, the investigation of superconductivity at the second magic angle would be of interest, as the strong orbital magnetic response could even lead to distinct Cooper pairing.

ACKNOWLEDGMENTS

The authors wish to thank E. Kaxiras, M. Luskin and Z. Zhu for useful discussions. The work of T.S. was supported by grant PID2020-113164GBI00 funded by MCIN/AEI/10.13039/501100011033, PID2023-146461NB-I00 funded by Ministerio de Ciencia, Innovación y Universidades as well as by the CSIC Research Platform on Quantum Technologies PTI-001. G.G-S. acknowledges support from the Spanish Ministry of Science, Innovation and Universities through the "María de Maeztu" Programme for Units of Excellence in R&D (CEX2023-001316-M).

Appendix A: Decoupling the N-layer Hamiltonian

Following Ref. 43, we consider the following Hamiltonian

$$H = \begin{bmatrix} H_1 & V & \dots & \dots & 0 \\ V^\dagger & H_2 & V & \dots & 0 \\ \vdots & \ddots & \ddots & \ddots & \vdots \\ 0 & \dots & V^\dagger & H_{N-1} & V \\ 0 & \dots & \dots & V^\dagger & H_N \end{bmatrix} . \tag{A1}$$

The $m \times m$-dimensional matrices H_ℓ and V denote the Hamiltonian of layer ℓ and the interlayer coupling, respectively.

Let us now set $H^{2\ell-1} = H_{\theta/2}$ and $H^{2\ell} = H_{-\theta/2}$ with $\ell = 1 \dots N/2$ and N even. For N odd, the decoupling procedure is equivalent, only with one additional decoupled single-layer Hamiltonian.

Rearranging the layers, we can write the Hamiltonian in the following way

$$H \to \begin{bmatrix} H^{N/2}_{\theta/2} & W \\ W^\dagger & H^{N/2}_{-\theta/2} \end{bmatrix} , \tag{A2}$$

with $H^{N/2}_{\pm\theta/2} = H_{\pm\theta/2} \otimes \mathbf{1}_{N/2}$ and $W = V \otimes C_{N/2}$ with

$$C_{N/2} = \begin{bmatrix} 1 & 0 & \dots & 0 \\ 1 & \ddots & \ddots & 0 \\ \vdots & \ddots & \ddots & \vdots \\ 0 & \dots & 1 & 1 \end{bmatrix} . \tag{A3}$$

We can now decompose the non-Hermitian matrix $C_{N/2}$ by its singular values, i.e., $C_{N/2} = A_{N/2} C^s_{N/2} B^\dagger_{N/2}$, where $C^s_{N/2} = \mathrm{diag}(\beta^k_N)$ with $(\beta^k_N)^2$ the eigenvalues of $C_{N/2}C^\dagger_{N/2}$. Furthermore, the columns of $A_{N/2}$ are the eigenvectors of $C_{N/2}C^\dagger_{N/2}$ and the columns of $B_{N/2}$ are the eigenvectors of $C^\dagger_{N/2}C_{N/2}$.

This decomposition now allows us to define the final unitary transformation $D = \mathrm{diag}(\mathbf{1}_m \otimes A_{N/2}, \mathbf{1}_m \otimes B_{N/2})$ to yield

$$H^s = D^\dagger H D = \begin{bmatrix} H^{N/2}_{\theta/2} & W^s \\ (W^s)^\dagger & H^{N/2}_{-\theta/2} \end{bmatrix} , \tag{A4}$$

where $W^s = V \otimes C^s_{N/2}$. Rearranging the Hamiltonian H^s, we thus arrive at a Hamiltonian that consists of the direct sum of twisted bilayer Hamiltonians with effective twist angles:

$$H \to \begin{bmatrix} H^{\mathrm{TBG}}_{\beta^1_N} & 0 & 0 & \dots & 0 \\ 0 & H^{\mathrm{TBG}}_{\beta^2_N} & 0 & \dots & 0 \\ \vdots & \ddots & \ddots & \ddots & \vdots \\ 0 & \dots & \dots & 0 & H^{\mathrm{TBG}}_{\beta^{N/2}_N} \end{bmatrix} , \tag{A5}$$

where $H^{\mathrm{TBG}}_{\beta^k_N}$ denotes the $2m \times 2m$-dimensional Hamiltonian of the twisted bilayer with renormalized interlayer hopping amplitude $(t^k_N)_\perp = \beta^k_N t_\perp$ with $\beta^k_N = 2\cos[\pi k/(N+1)]$, $k = 1, ..., N/2$ [43]. For small initial twist angle θ and few layers, this is equivalent to the renormalization of the twist angle of the multilayer system, $\theta^k_{N,m} = \beta^k_N \theta_m$ [3].

Appendix B: Transformation of the current operators

1. Tetralayer transformation

For a system with four layers, the matrices that yield the singular value decomposition read

$$A = \frac{5^{-1/4}}{\sqrt{\varphi}} \begin{bmatrix} 1 & -\varphi \\ \varphi & 1 \end{bmatrix} , B = \frac{5^{-1/4}}{\sqrt{\varphi}} \begin{bmatrix} \varphi & -1 \\ 1 & \varphi \end{bmatrix} , \tag{B1}$$

where $\varphi = (1+\sqrt{5})/2$. Reordering the Hamiltonian again, we obtain the unitary matrix that block-diagonalizes the Hamiltonian, i.e.,

$$H \to T^\dagger H T = \begin{pmatrix} H^{\mathrm{TBG}}_{\varphi} & 0 \\ 0 & H^{\mathrm{TBG}}_{\varphi^{-1}} \end{pmatrix} , \tag{B2}$$

where H^{TBG}_β is the Hamiltonian of the twisted bilayer with the two renormalized interlayer coupling amplitudes $(t^k_N)_\perp = \beta^k_4 t_\perp$. The effective twist angle can therefore be approximated by $\theta^k_4 = \beta^k_4 \theta_m$, so that the first two magic angles read $\theta^1_{4,m} = \varphi\theta_m \approx 1.70^\circ$ and $\theta^2_{4,m} = \varphi^{-1}\theta_m \approx 0.65^\circ$, with $\theta_m = 1.05^\circ$.

The unitary matrix is

$$T = \frac{5^{-1/4}}{\sqrt{\varphi}} \begin{pmatrix} 1 & 0 & -\varphi & 0 \\ 0 & \varphi & 0 & -1 \\ \varphi & 0 & 1 & 0 \\ 0 & 1 & 0 & \varphi \end{pmatrix} , \tag{B3}$$

where each component is proportional to the $m \times m$-unity matrix, with $m = 2$ in the case of an underlying continuum model or $m = 2A_M$ in the case of a tight-binding model with commensurate twist angle $\theta = \arccos[1 - 1/(2A_M)]$, where $A_M = 3M^3 + 3M + 1$. This matrix relates the initial layer operators c_ℓ to the transformed layer operators $\bar{c}_\ell$:

$$c_1 = \frac{5^{-1/4}}{\sqrt{\varphi}} (\bar{c}_1 - \varphi \bar{c}_3) , \tag{B4}$$

$$c_2 = \frac{5^{-1/4}}{\sqrt{\varphi}} (\varphi \bar{c}_2 - \bar{c}_4) , \tag{B5}$$

$$c_3 = \frac{5^{-1/4}}{\sqrt{\varphi}} (\varphi \bar{c}_1 + \bar{c}_3) , \tag{B6}$$

$$c_4 = \frac{5^{-1/4}}{\sqrt{\varphi}} (\bar{c}_2 + \varphi \bar{c}_4) . \tag{B7}$$

The layer current is now related to the bilinear combination of the layer operators $j_{\ell\ell} \propto c_\ell^\dagger c_\ell$. Note that we could have omitted the second layer index $j_{\ell\ell} \to j_\ell$ as we only discuss in-plane sheet current densities. This current can now be related to the transformed current $\bar{j}_{\ell\ell'} \propto \bar{c}_\ell^\dagger \bar{c}_{\ell'}$ as follows:

$$j_{11} = \frac{5^{-1/2}}{\varphi}[\bar{j}_{11} + \varphi^2 \bar{j}_{33} - \varphi(\bar{j}_{13} + \bar{j}_{31})] \,, \tag{B8}$$

$$j_{22} = \frac{5^{-1/2}}{\varphi}[\varphi^2 \bar{j}_{22} + \bar{j}_{44} - \varphi(\bar{j}_{24} + \bar{j}_{42})] \,, \tag{B9}$$

$$j_{33} = \frac{5^{-1/2}}{\varphi}[\varphi^2 \bar{j}_{11} + \bar{j}_{33} + \varphi(\bar{j}_{13} + \bar{j}_{31})] \,, \tag{B10}$$

$$j_{44} = \frac{5^{-1/2}}{\varphi}[\bar{j}_{22} + \varphi^2 \bar{j}_{44} + \varphi(\bar{j}_{24} + \bar{j}_{42})] \,. \tag{B11}$$

The ten correlation functions can now be written explicitly in terms of the transformed currents as follows:

$$\langle\langle j_{11} j_{11}\rangle\rangle = \frac{1}{5\varphi^2}\Big[\langle\langle \bar{j}_{11}\bar{j}_{11}\rangle\rangle + \varphi^4\langle\langle \bar{j}_{33}\bar{j}_{33}\rangle\rangle + \varphi^2\langle\langle \bar{j}_{13}\bar{j}_{31} + \bar{j}_{31}\bar{j}_{13}\rangle\rangle\Big] \,, \tag{B12}$$

$$\langle\langle j_{11} j_{22}\rangle\rangle = \frac{1}{5\varphi^2}\Big[\varphi^2\langle\langle \bar{j}_{11}\bar{j}_{22}\rangle\rangle + \varphi^2\langle\langle \bar{j}_{33}\bar{j}_{44}\rangle\rangle + \varphi^2\langle\langle \bar{j}_{13}\bar{j}_{42} + \bar{j}_{31}\bar{j}_{24}\rangle\rangle\Big] \,, \tag{B13}$$

$$\langle\langle j_{11} j_{33}\rangle\rangle = \frac{1}{5\varphi^2}\Big[\varphi^2\langle\langle \bar{j}_{11}\bar{j}_{11}\rangle\rangle + \varphi^2\langle\langle \bar{j}_{33}\bar{j}_{33}\rangle\rangle - \varphi^2\langle\langle \bar{j}_{13}\bar{j}_{31} + \bar{j}_{31}\bar{j}_{13}\rangle\rangle\Big] \,, \tag{B14}$$

$$\langle\langle j_{11} j_{44}\rangle\rangle = \frac{1}{5\varphi^2}\Big[\langle\langle \bar{j}_{11}\bar{j}_{22}\rangle\rangle + \varphi^4\langle\langle \bar{j}_{33}\bar{j}_{44}\rangle\rangle - \varphi^2\langle\langle \bar{j}_{13}\bar{j}_{42} + \bar{j}_{31}\bar{j}_{24}\rangle\rangle\Big] \tag{B15}$$

$$\langle\langle j_{22} j_{22}\rangle\rangle = \frac{1}{5\varphi^2}\Big[\varphi^4\langle\langle \bar{j}_{22}\bar{j}_{22}\rangle\rangle + \langle\langle \bar{j}_{44}\bar{j}_{44}\rangle\rangle + \varphi^2\langle\langle \bar{j}_{24}\bar{j}_{42} + \bar{j}_{42}\bar{j}_{24}\rangle\rangle\Big] \,, \tag{B16}$$

$$\langle\langle j_{22} j_{33}\rangle\rangle = \frac{1}{5\varphi^2}\Big[\varphi^4\langle\langle \bar{j}_{22}\bar{j}_{11}\rangle\rangle + \langle\langle \bar{j}_{44}\bar{j}_{33}\rangle\rangle - \varphi^2\langle\langle \bar{j}_{24}\bar{j}_{31} + \bar{j}_{42}\bar{j}_{13}\rangle\rangle\Big] \,, \tag{B17}$$

$$\langle\langle j_{22} j_{44}\rangle\rangle = \frac{1}{5\varphi^2}\Big[\varphi^2\langle\langle \bar{j}_{22}\bar{j}_{22}\rangle\rangle + \varphi^2\langle\langle \bar{j}_{44}\bar{j}_{44}\rangle\rangle - \varphi^2\langle\langle \bar{j}_{24}\bar{j}_{42} + \bar{j}_{42}\bar{j}_{24}\rangle\rangle\Big] \,, \tag{B18}$$

$$\langle\langle j_{33} j_{33}\rangle\rangle = \frac{1}{5\varphi^2}\Big[\varphi^4\langle\langle \bar{j}_{11}\bar{j}_{11}\rangle\rangle + \langle\langle \bar{j}_{33}\bar{j}_{33}\rangle\rangle + \varphi^2\langle\langle \bar{j}_{13}\bar{j}_{31} + \bar{j}_{31}\bar{j}_{13}\rangle\rangle\Big] \,, \tag{B19}$$

$$\langle\langle j_{33} j_{44}\rangle\rangle = \frac{1}{5\varphi^2}\Big[\varphi^2\langle\langle \bar{j}_{11}\bar{j}_{22}\rangle\rangle + \varphi^2\langle\langle \bar{j}_{33}\bar{j}_{44}\rangle\rangle + \varphi^2\langle\langle \bar{j}_{13}\bar{j}_{42} + \bar{j}_{31}\bar{j}_{24}\rangle\rangle\Big] \,, \tag{B20}$$

$$\langle\langle j_{44} j_{44}\rangle\rangle = \frac{1}{5\varphi^2}\Big[\langle\langle \bar{j}_{22}\bar{j}_{22}\rangle\rangle + \varphi^4\langle\langle \bar{j}_{44}\bar{j}_{44}\rangle\rangle + \varphi^2\langle\langle \bar{j}_{24}\bar{j}_{42} + \bar{j}_{42}\bar{j}_{24}\rangle\rangle\Big] \,. \tag{B21}$$

These correlators allow one to express the magnetic susceptibilities of the tetralayer system in terms of the ones of TBG, given by Eqs. (22-25). This yields

$$\sigma_0^{11} = \frac{1}{5}\left[\varphi^{-2}\sigma_0^1 + \varphi^2\sigma_0^2 + \sigma_c^1\right] \,, \tag{B22}$$

$$\sigma_0^{12} = \frac{1}{5}\left[\sigma_1^1 + \sigma_1^2 + \sigma_c^3\right] \,, \tag{B23}$$

$$\sigma_0^{13} = \frac{1}{5}\left[\sigma_0^1 + \sigma_0^2 - \sigma_c^1\right] \,, \tag{B24}$$

$$\sigma_0^{14} = \frac{1}{5}\left[\varphi^{-2}\sigma_1^1 + \varphi^2\sigma_1^2 - \sigma_c^3\right] \,, \tag{B25}$$

$$\sigma_0^{22} = \frac{1}{5}\left[\varphi^2\sigma_0^1 + \varphi^{-2}\sigma_0^2 + \sigma_c^2\right] \,, \tag{B26}$$

$$\sigma_0^{23} = \frac{1}{5}\left[\varphi^2\sigma_1^1 + \varphi^{-2}\sigma_1^2 - \sigma_c^3\right] \,, \tag{B27}$$

$$\sigma_0^{24} = \frac{1}{5}\left[\sigma_0^1 + \sigma_0^2 - \sigma_c^2\right] \,, \tag{B28}$$

$$\sigma_0^{33} = \frac{1}{5}\left[\varphi^2\sigma_0^1 + \varphi^{-2}\sigma_0^2 + \sigma_c^1\right] \,, \tag{B29}$$

$$\sigma_0^{34} = \frac{1}{5}\left[\sigma_1^1 + \sigma_1^2 + \sigma_c^3\right] \,, \tag{B30}$$

$$\sigma_0^{44} = \frac{1}{5}\left[\varphi^{-2}\sigma_0^1 + \varphi^2\sigma_0^2 + \sigma_c^2\right] \,. \tag{B31}$$

These expressions allow one to compute the magnetic susceptibilities of the tetralayer system.

2. Pentalayer transformation

Following Ref. 43, we start from the unitary transformation that block-diagonalizes the Hamiltonian, i.e.

$$H = \boldsymbol{T}^\dagger H \boldsymbol{T} = \begin{pmatrix} H_{\sqrt{3}}^{\mathrm{TBG}} & 0 & 0 \\ 0 & H_1^{\mathrm{TBG}} & 0 \\ 0 & 0 & H^{\mathrm{SLG}} \end{pmatrix} \,, \tag{B32}$$

where H_β^{TBG} is the Hamiltonian of TBG with the two renormalized interlayer coupling amplitudes $(t_N^k)_\perp = \beta_4^k t_\perp$ and H^{SLG} the Hamiltonian of a monolayer graphene. The effective twist angles are approximated by $\theta_{5,m}^k = \beta_5^k \theta_m$, giving $\theta_{5,m}^1 = \sqrt{3}\theta_m \approx 1.87°$ and $\theta_{5,m}^2 = \theta_m \approx 1.05°$, with θ_2 the magic angle of TBG.

The original layer operators c_ℓ are related to the transformed operators $\bar{c}_\ell$ as:

$$c_1 = \frac{1}{\sqrt{6}}(\bar{c}_1 - \sqrt{3}\bar{c}_3 + \sqrt{2}\bar{c}_5) \,, \tag{B33}$$

$$c_2 = \frac{1}{\sqrt{2}}(\bar{c}_2 - \bar{c}_4) \,, \tag{B34}$$

$$c_3 = \frac{1}{\sqrt{3}}(\sqrt{2}\bar{c}_1 - \bar{c}_5) \,, \tag{B35}$$

$$c_4 = \frac{1}{\sqrt{2}}(\bar{c}_2 + \bar{c}_4) \,, \tag{B36}$$

$$c_5 = \frac{1}{\sqrt{6}}(\bar{c}_1 + \sqrt{3}\bar{c}_3 + \sqrt{2}\bar{c}_5) \,. \tag{B37}$$

The layer current is again related to the bilinear combination of the layer operators $j_{\ell\ell} \propto c_\ell^\dagger c_\ell$. Note that the second layer index may be omitted, $j_{\ell\ell} \to j_\ell$, since we only consider in-plane sheet current densities. This current can now be related to the transformed current $\bar{j}_{\ell\ell'} \propto \bar{c}_\ell^\dagger \bar{c}_{\ell'}$ as follows:

$$\begin{aligned} j_{11} = \frac{1}{6}(&\bar{j}_{11} + 3\bar{j}_{33} + 2\bar{j}_{55} - \sqrt{3}(\bar{j}_{13} + \bar{j}_{31}) \\ &+ \sqrt{2}(\bar{j}_{15} + \bar{j}_{51}) - \sqrt{6}(\bar{j}_{35} + \bar{j}_{53})) \,, \end{aligned} \tag{B38}$$

$$j_{22} = \frac{1}{2}(\bar{j}_{22} + \bar{j}_{44} - (\bar{j}_{24} + \bar{j}_{42})) \,, \tag{B39}$$

$$j_{33} = \frac{1}{3}(2\bar{j}_{11} + \bar{j}_{55} - \sqrt{2}(\bar{j}_{15} + \bar{j}_{51})) \,, \tag{B40}$$

$$j_{44} = \frac{1}{2}(\bar{j}_{22} + \bar{j}_{44} + (\bar{j}_{24} + \bar{j}_{42})) \,, \tag{B41}$$

$$\begin{aligned} j_{55} = \frac{1}{6}(&\bar{j}_{11} + 3\bar{j}_{33} + 2\bar{j}_{55} + \sqrt{3}(\bar{j}_{13} + \bar{j}_{31}) \\ &+ \sqrt{2}(\bar{j}_{15} + \bar{j}_{51}) + \sqrt{6}(\bar{j}_{35} + \bar{j}_{53})) \,. \end{aligned} \tag{B42}$$

The fifteen correlators can now be expressed in terms of the transformed currents. Using the same notation as in the tetralayer case, the layer-discriminated conductivities are related to the two effective TBG systems through Eqs. (22-25). In addition, we introduce $\sigma_0^3 = \langle\langle \bar{j}_{55}\bar{j}_{55}\rangle\rangle$ to denote the conductivity of the decoupled single-layer graphene. The couplings between the effective systems are described by

$$\sigma_c^1 = \langle\langle \bar{j}_{13}\bar{j}_{31} + \bar{j}_{31}\bar{j}_{13}\rangle\rangle, \tag{B43}$$

$$\sigma_c^2 = \langle\langle \bar{j}_{24}\bar{j}_{42} + \bar{j}_{42}\bar{j}_{24}\rangle\rangle, \tag{B44}$$

$$\sigma_c^3 = \langle\langle \bar{j}_{15}\bar{j}_{51} + \bar{j}_{51}\bar{j}_{15}\rangle\rangle, \tag{B45}$$

$$\sigma_c^4 = \langle\langle \bar{j}_{35}\bar{j}_{53} + \bar{j}_{53}\bar{j}_{35}\rangle\rangle, \tag{B46}$$

$$\sigma_c^5 = \langle\langle \bar{j}_{13}\bar{j}_{42} + \bar{j}_{31}\bar{j}_{24}\rangle\rangle \;= \langle\langle \bar{j}_{24}\bar{j}_{31} + \bar{j}_{42}\bar{j}_{13}\rangle\rangle. \tag{B47}$$

The correlators finally read:

$$\sigma_0^{11} = \frac{1}{36}\left[\sigma_0^1 + 9\sigma_0^2 + 4\sigma_0^3 + 3\sigma_c^1 + 2\sigma_c^3 + 6\sigma_c^4\right] \,, \tag{B48}$$

$$\sigma_0^{12} = \frac{1}{12}\left[\sigma_1^1 + 3\sigma_1^2 + \sqrt{3}\sigma_c^5\right] \,, \tag{B49}$$

$$\sigma_0^{13} = \frac{1}{9}\left[\sigma_0^1 + \sigma_0^3 - \sigma_c^3\right] \,, \tag{B50}$$

$$\sigma_0^{14} = \frac{1}{12}\left[\sigma_1^1 + 3\sigma_1^2 - \sqrt{3}\sigma_c^5\right] \,, \tag{B51}$$

$$\sigma_0^{15} = \frac{1}{36}\left[\sigma_0^1 + 9\sigma_0^2 + 4\sigma_0^3 - 3\sigma_c^1 + 2\sigma_c^3 - 6\sigma_c^4\right] \,, \tag{B52}$$

$$\sigma_0^{22} = \frac{1}{4}\left[\sigma_0^1 + \sigma_0^2 + \sigma_c^2\right] \,, \tag{B53}$$

$$\sigma_0^{23} = \frac{1}{3}\sigma_1^1 \,, \tag{B54}$$

$$\sigma_0^{24} = \frac{1}{4}\left[\sigma_0^1 + \sigma_0^2 - \sigma_c^2\right] \,, \tag{B55}$$

$$\sigma_0^{25} = \frac{1}{12}\left[\sigma_1^1 + 3\sigma_1^2 - \sqrt{3}\sigma_c^5\right] \,, \tag{B56}$$

$$\sigma_0^{33} = \frac{1}{9}\left[4\sigma_0^1 + \sigma_0^3 + 2\sigma_c^3\right] \,, \tag{B57}$$

$$\sigma_0^{34} = \frac{1}{3}\sigma_1^1 \,, \tag{B58}$$

$$\sigma_0^{35} = \frac{1}{9}\left[\sigma_0^1 + \sigma_0^3 - \sigma_c^3\right] \,, \tag{B59}$$

$$\sigma_0^{44} = \frac{1}{4}\left[\sigma_0^1 + \sigma_0^2 + \sigma_c^2\right] \,, \tag{B60}$$

$$\sigma_0^{45} = \frac{1}{12}\left[\sigma_1^1 + 3\sigma_1^2 + \sqrt{3}\sigma_c^5\right] \,, \tag{B61}$$

$$\sigma_0^{55} = \frac{1}{36}\left[\sigma_0^1 + 9\sigma_0^2 + 4\sigma_0^3 + 3\sigma_c^1 + 2\sigma_c^3 + 6\sigma_c^4\right] \,. \tag{B62}$$

These expressions allow one to compute the magnetic susceptibilities of the pentalayer system.

[1] Y. Cao, V. Fatemi, S. Fang, K. Watanabe, T. Taniguchi, E. Kaxiras, and P. Jarillo-Herrero, Unconventional superconductivity in magic-angle graphene superlattices, Nature **556**, 43 (2018).

[2] E. Suárez Morell, J. D. Correa, P. Vargas, M. Pacheco, and Z. Barticevic, Flat bands in slightly twisted bilayer graphene: Tight-binding calculations, Phys. Rev. B **82**, 121407 (2010).

[3] R. Bistritzer and A. H. MacDonald, Moiré bands in twisted double-layer graphene, Proc. Natl. Acad. Sci. (USA) **108**, 12233 (2011).

[4] S. Carr, D. Massatt, S. Fang, P. Cazeaux, M. Luskin, and E. Kaxiras, Twistronics: Manipulating the electronic properties of two-dimensional layered structures through their twist angle, Physical Review B **95**, 075420 (2017).

[5] Y. Cao, V. Fatemi, A. Demir, S. Fang, S. L. Tomarken, J. Y. Luo, J. D. Sanchez-Yamagishi, K. Watanabe, T. Taniguchi, E. Kaxiras, R. C. Ashoori, and P. Jarillo-Herrero, Correlated insulator behaviour at half-filling in magic-angle graphene superlattices, Nature **556**, 80 (2018).

[6] B. L. Chittari, N. Leconte, S. Javvaji, and J. Jung, Pressure induced compression of flatbands in twisted bilayer graphene, Electronic Structure **1**, 015001 (2018).

[7] H. Isobe, N. F. Yuan, and L. Fu, Unconventional superconductivity and density waves in twisted bilayer graphene, Physical Review X **8**, 041041 (2018).

[8] D. M. Kennes, J. Lischner, and C. Karrasch, Strong correlations and d+id superconductivity in twisted bilayer graphene, Physical Review B **98**, 241407 (2018).

[9] M. Koshino, N. F. Yuan, T. Koretsune, M. Ochi, K. Kuroki, and L. Fu, Maximally localized wannier orbitals and the extended hubbard model for twisted bilayer graphene, Physical Review X **8**, 031087 (2018).

[10] L. Zou, H. C. Po, A. Vishwanath, and T. Senthil, Band structure of twisted bilayer graphene: Emergent symmetries, commensurate approximants, and wannier obstructions, Physical Review B **98**, 085435 (2018).

[11] J. González and T. Stauber, Kohn-luttinger superconductivity in twisted bilayer graphene, Physical Review Letters **122**, 026801 (2019).

[12] J. Kang and O. Vafek, Strong coupling phases of partially filled twisted bilayer graphene narrow bands, Physical Review Letters **122**, 246401 (2019).

[13] B. Lian, Z. Wang, and B. A. Bernevig, Twisted bilayer graphene: A phonon-driven superconductor, Physical Review Letters **122**, 257002 (2019).

[14] H. Polshyn, M. Yankowitz, S. Chen, Y. Zhang, K. Watanabe, T. Taniguchi, C. R. Dean, and A. F. Young, Large linear-in-temperature resistivity in twisted bilayer graphene, Nature Physics **15**, 1011 (2019).

[15] B. Roy and V. Juričić, Unconventional superconductivity in nearly flat bands in twisted bilayer graphene, Physical Review B **99**, 121407 (2019).

[16] Y.-H. Zhang, D. Mao, Y. Cao, P. Jarillo-Herrero, and T. Senthil, Nearly flat chern bands in moiré superlattices, Physical Review B **99**, 075127 (2019).

[17] Y. Cao, D. Chowdhury, D. Rodan-Legrain, O. Rubies-Bigorda, K. Watanabe, T. Taniguchi, T. Senthil, and P. Jarillo-Herrero, Strange metal in magic-angle graphene with near planckian dissipation, Physical Review Letters **124**, 076801 (2020).

[18] D. V. Chichinadze, L. Classen, and A. V. Chubukov, Nematic superconductivity in twisted bilayer graphene, Physical Review B **101**, 224513 (2020).

[19] K. P. Nuckolls, M. Oh, D. Wong, B. Lian, K. Watanabe, T. Taniguchi, B. A. Bernevig, and A. Yazdani, Strongly correlated chern insulators in magic-angle twisted bilayer graphene, Nature **588**, 610 (2020).

[20] Y. Saito, J. Ge, K. Watanabe, T. Taniguchi, and A. F. Young, Independent superconductors and correlated insulators in twisted bilayer graphene, Nature Physics **16**, 926 (2020).

[21] B. Lian, Z.-D. Song, N. Regnault, D. K. Efetov, A. Yazdani, and B. A. Bernevig, Twisted bilayer graphene. iv. exact insulator ground states and phase diagram, Physical Review B **103**, 205414 (2021).

[22] Y. Saito, F. Yang, J. Ge, X. Liu, T. Taniguchi, K. Watanabe, J. I. A. Li, E. Berg, and A. F. Young, Isospin pomeranchuk effect in twisted bilayer graphene, Nature **592**, 220 (2021).

[23] Y. Xie, A. T. Pierce, J. M. Park, D. E. Parker, E. Khalaf, P. Ledwith, Y. Cao, S. H. Lee, S. Chen, P. R. Forrester, K. Watanabe, T. Taniguchi, A. Vishwanath, P. Jarillo-Herrero, and A. Yacoby, Fractional Chern insulators in magic-angle twisted bilayer graphene, Nature **600**, 439 (2021).

[24] G. Di Battista, P. Seifert, K. Watanabe, T. Taniguchi, K. C. Fong, A. Principi, and D. K. Efetov, Revealing the thermal properties of superconducting magic-angle twisted bilayer graphene, Nano Letters **22**, 6465 (2022).

[25] A. Jaoui, I. Das, G. Di Battista, J. Díez-Mérida, X. Lu, K. Watanabe, T. Taniguchi, H. Ishizuka, L. Levitov, and D. K. Efetov, Quantum critical behaviour in magic-angle twisted bilayer graphene, Nature Physics **18**, 633 (2022).

[26] Z. Dong, L. Levitov, and A. V. Chubukov, Superconductivity near spin and valley orders in graphene multilayers, Physical Review B **108**, 134503 (2023).

[27] J. Ingham, T. Li, M. S. Scheurer, and H. D. Scammell, Quadratic dirac fermions and the competition of ordered states in twisted bilayer graphene (2023).

[28] Y.-Z. Chou, Y. Tan, F. Wu, and S. Das Sarma, Topological flat bands, valley polarization, and interband superconductivity in magic-angle twisted bilayer graphene with proximitized spin-orbit couplings, Physical Review B **110**, l041108 (2024).

[29] G. Rai, L. Crippa, D. Călugăru, H. Hu, F. Paoletti, L. de' Medici, A. Georges, B. A. Bernevig, R. Valentí, G. Sangiovanni, and T. Wehling, Dynamical correlations and order in magic-angle twisted bilayer graphene, Physical Review X **14**, 031045 (2024).

[30] Y.-J. Wang, G.-D. Zhou, S.-Y. Peng, B. Lian, and Z.-D. Song, Molecular pairing in twisted bilayer

graphene superconductivity, Physical Review Letters **133**, 146001 (2024).
[31] G.-D. Zhou, Y.-J. Wang, N. Tong, and Z.-D. Song, Kondo phase in twisted bilayer graphene, Physical Review B **109**, 045419 (2024).
[32] R. Dutta, A. Ghosh, S. Mandal, K. Watanabe, T. Taniguchi, H. R. Krishnamurthy, S. Banerjee, M. Jain, and A. Das, Electric field-tunable superconductivity with competing orders in twisted bilayer graphene near the magic angle, ACS Nano **19**, 5353 (2025).
[33] J. M. Park, S. Sun, K. Watanabe, T. Taniguchi, and P. Jarillo-Herrero, Experimental evidence for nodal superconducting gap in moiré graphene, Science **391**, 79 (2026).
[34] E. Y. Andrei and A. H. MacDonald, Graphene bilayers with a twist, Nat. Mater. **19**, 1265 (2020).
[35] M. Yankowitz, S. Chen, H. Polshyn, Y. Zhang, K. Watanabe, T. Taniguchi, D. Graf, A. F. Young, and C. R. Dean, Tuning superconductivity in twisted bilayer graphene, Science **363**, 1059 (2019).
[36] L. Balents, C. R. Dean, D. K. Efetov, and A. F. Young, Superconductivity and strong correlations in moiré flat bands, Nature Physics **16**, 725 (2020).
[37] J. M. Park, Y. Cao, K. Watanabe, T. Taniguchi, and P. Jarillo-Herrero, Tunable strongly coupled superconductivity in magic-angle twisted trilayer graphene, Nature **590**, 249 (2021).
[38] Z. Hao, A. M. Zimmerman, P. Ledwith, E. Khalaf, D. H. Najafabadi, K. Watanabe, T. Taniguchi, A. Vishwanath, and P. Kim, Electric field-tunable superconductivity in alternating-twist magic-angle trilayer graphene, Science **371**, 1133 (2021).
[39] Y. Cao, J. M. Park, K. Watanabe, T. Taniguchi, and P. Jarillo-Herrero, Pauli-limit violation and re-entrant superconductivity in moiré graphene, Nature **595**, 526 (2021).
[40] H. Kim, Y. Choi, É. Lantagne-Hurtubise, C. Lewandowski, A. Thomson, L. Kong, H. Zhou, E. Baum, Y. Zhang, L. Holleis, K. Watanabe, T. Taniguchi, A. F. Young, J. Alicea, and S. Nadj-Perge, Imaging inter-valley coherent order in magic-angle twisted trilayer graphene, Nature **623**, 942 (2023).
[41] A. Uri, S. C. de la Barrera, M. T. Randeria, D. Rodan-Legrain, T. Devakul, P. J. D. Crowley, N. Paul, K. Watanabe, T. Taniguchi, R. Lifshitz, L. Fu, R. C. Ashoori, and P. Jarillo-Herrero, Superconductivity and strong interactions in a tunable moiré quasicrystal, Nature **620**, 762 (2023).
[42] L.-Q. Xia, S. C. de la Barrera, A. Uri, A. Sharpe, Y. H. Kwan, Z. Zhu, K. Watanabe, T. Taniguchi, D. Goldhaber-Gordon, L. Fu, T. Devakul, and P. Jarillo-Herrero, Helical trilayer graphene: A moiré platform for strongly-interacting topological bands, e-print , arXiv:2310.12204v1 [cond-mat.mes-hall] (2023).
[43] E. Khalaf, A. J. Kruchkov, G. Tarnopolsky, and A. Vishwanath, Magic angle hierarchy in twisted graphene multilayers, Phys. Rev. B **100**, 085109 (2019).
[44] A. M. Clogston, Upper limit for the critical field in hard superconductors, Phys. Rev. Lett. **9**, 266 (1962).
[45] B. S. Chandrasekhar, A note on the maximum critical field of high-field superconductors, Appl. Phys. Lett. **1**, 7 (1962).
[46] J. M. Park, Y. Cao, L.-Q. Xia, S. Sun, K. Watanabe, T. Taniguchi, and P. Jarillo-Herrero, Robust superconductivity in magic-angle multilayer graphene family, Nat. Mater. **21**, 877 (2022).
[47] P. J. Ledwith, A. Vishwanath, and E. Khalaf, Family of ideal Chern flatbands with arbitrary Chern number in chiral twisted graphene multilayers, Phys. Rev. Lett. **128**, 176404 (2022).
[48] E. Lake and T. Senthil, Reentrant superconductivity through a quantum lifshitz transition in twisted trilayer graphene, Physical Review B **104**, 174505 (2021).
[49] M. Christos, S. Sachdev, and M. S. Scheurer, Correlated insulators, semimetals, and superconductivity in twisted trilayer graphene, Phys. Rev. X **12**, 021018 (2022).
[50] J. M. Park, S. Sun, K. Watanabe, T. Taniguchi, and P. Jarillo-Herrero, Experimental evidence for nodal superconducting gap in moiré graphene, Science **391**, 79 (2026).
[51] T. Stauber, T. Low, and G. Gómez-Santos, Chiral response of twisted bilayer graphene, Phys. Rev. Lett. **120**, 046801 (2018).
[52] D. Guerci, P. Simon, and C. Mora, Moiré lattice effects on the orbital magnetic response of twisted bilayer graphene and Condon instability, Phys. Rev. B **103**, 224436 (2021).
[53] T. Stauber, M. Wackerl, P. Wenk, D. Margetis, J. González, G. Gómez-Santos, and J. Schliemann, Neutral magic-angle bilayer graphene: Condon instability and chiral resonances, Small Sci. **3**, 2200080 (2023).
[54] W.-Y. He, D. Goldhaber-Gordon, and K. T. Law, Giant orbital magnetoelectric effect and current-induced magnetization switching in twisted bilayer graphene, Nature Communications **11**, 10.1038/s41467-020-15473-9 (2020).
[55] O. Antebi, A. Stern, and E. Berg, In-plane orbital magnetization as a probe for symmetry breaking in strained twisted bilayer graphene, Physical Review B **105**, 104423 (2022).
[56] D. Margetis, G. Gómez-Santos, and T. Stauber, Optical response of alternating twisted trilayer graphene, Phys. Rev. B **110**, 205144 (2024).
[57] T. Stauber, T. Low, and G. Gómez-Santos, Linear response of twisted bilayer graphene: Continuum versus tight-binding models, Phys. Rev. B **98**, 195414 (2018).
[58] D. J. Scalapino, S. R. White, and S. Zhang, Insulator, metal, or superconductor: The criteria, Phys. Rev. B **47**, 7995 (1993).
[59] M. Sánchez Sánchez, I. Díaz, J. González, and T. Stauber, Nematic versus kekulé phases in twisted bilayer graphene under hydrostatic pressure, Phys. Rev. Lett. **133**, 266603 (2024).
[60] K. Maki, Effect of pauli paramagnetism on magnetic properties of high-field superconductors, Phys. Rev. **148**, 362 (1966).